24th COBEM - 2017

24th ABCM International Congress of Mechanical Engineering
December 3-8, 2017, Curitiba, PR, Brazil

COBEM-2017-2118
A SHELL BASED FEM MODEL FOR THICK WALLED COMPOSITE ROTORS

Vergílio Torezan Silingardi Del Claro
Paulo Costa Porto de Figueiredo Barbosa
LMEst - Laboratory of Mechanics and Structures, Federal University of Uberlândia, School of Mechanical Engineering, Av. João Naves de Ávila, 2121, Uberlândia, MG, 38408-196, Brazil.
vergilio.claro@ufu.br, paulo.barbosa@ufu.br
Aldemir Ap Cavalini Jr
LMEst - Laboratory of Mechanics and Structures, Federal University of Uberlândia, School of Mechanical Engineering, Av. João Naves de Ávila, 2121, Uberlândia, MG, 38408-196, Brazil.
aacjunior@ufu.br;
Valder Steffen Jr
LMEst - Laboratory of Mechanics and Structures, Federal University of Uberlândia, School of Mechanical Engineering, Av. João Naves de Ávila, 2121, Uberlândia, MG, 38408-196, Brazil.
vsteffen@ufu.br.

Abstract. *In the present contribution, a shell based FEM formulation is used in the context of a numerical investigation regarding the dynamic behavior of a free-free composite thick-walled hollow shaft. For this aim, a flexible composite shaft forms the considered system. The mathematical model of the rotor is derived from the FSDT theory developed with additional stiffness terms, in pair with a shell based formulation. Special emphasis is given to the modelling and experimental determination of the modal damping factors. In this study, a convergence procedure is carried out for the adjustment of critical parameters using an optimization procedure comparing the experimental and numerical FRFs to obtain a representative model for the rotor system. In addition, another objective of this study is the development of a straightforward strategy for the determination of the physical properties of mechanical components as, based on inverse problem approach through optimization techniques. Finally, the present study discusses the convenience of composite hollow shafts for rotor dynamics applications.*

Keywords: *composites, rotor dynamics, shell, finite elements method, composite material shaft.*

1. INTRODUCTION

Rotor dynamics is a well-developed field of science and engineering, having been studied for over 140 years (Ishida and Yamamoto, 2012). Among the many contributions to this field, many models were employed with the objective of better representing the dynamic behavior of rotating machineries. Historically, while modelling subcritical rotors, these were considered rigid, allowing for relatively simple approaches to yield accurate results. Once supercritical rotors started being used, some new theories were developed to properly consider the more complex dynamic effects that appeared, such as the transfer matrix method (Lallement *et al.*, 1982) and the finite elements method (FEM), which was firstly used in rotor dynamic by (Nelson and Macvaugh, 1979). More recently, with composite shaft rotor systems being increasingly used in industrial applications, some new models and/or modifications to existing ones became necessary, for many of the simplifications made for metallic shafts incur into inaccurate approximations while modelling composites.

Composite rotors and shafts are commercially used by major companies, such as Mazda Motor Corp. in the vehicle *Cardan* shafts, Airbus, Bombardier, Boeing and others, as shafts for control surfaces actuating system and by almost all modern helicopter manufacturers, in the rotor blades (Crompton Technology Group, 2015). These composite shafts have a number of intrinsic advantages over their metallic counterparts, being the most evident its overwhelmingly better structural efficiency. Other specificities of composite materials are due to the fabrication process, made by lamination of a multitude of fibrous layers embedded on a rigid resin matrix. The fibrous part of the composite is generally made of Carbon Fibers, for general engineering applications, and Kevlar®, fiberglass and others, depending on project pre-requisites. As for the resin, it is usually composed by epoxy with different properties for each situation and, in some cases, can be composed by a number of different polymers. The widely variable composition of both the matrix and the

fibers, as well as the stacking sequence of the layers, fiber orientations in layer orthogonality and fiber-matrix interface, produces some complicating effects that interfere in the operation of composite components.

With the intent of properly representing these components, many contributions have been made in the study of composite materials and their mechanical behavior under loading condition. More specifically, composite rotors have also been recently studied with emphasis on modelling the dynamic effects of rotating machinery with composite specificities. Such studies are exemplified by (Singh and Gupta, 1996a), which used equivalent modulus and layer-wise beam theories along a Rayleigh-Ritz formulation to model a composite rotor. An improvement over this model came with (Chatelet *et al*, 2002), representing a multilayered composite rotor in terms of its mode shapes. Posterior studies on the influence of the stacking sequence on composites was addressed by (Sino *et al*, 2008), followed by a comparison on performance and structural damping for different composites constitutions (Alwan *et al*, 2010). More recently, composite rotors with embedded shape memory alloy (SMA) wires were studied by (Ren *et al*, 2014), and the dynamic behavior of hollow composite shafts by (Cavalini *et al*, 2017).

Among the many recent contributions to the study of composite rotating machinery, the present work presents a shell based Finite Element Method (FEM) formulation for the modeling of multi-layered composite hollow shafts. The model accuracy is supported by experimental validation of the numeric results, as well as a numerical comparison between the current proposed model and other simpler ones, already experimentally validated.

2. NUMERICAL AND EXPERIMENTAL PROCEDURES

Focusing on the development of a numeric procedure to represent the dynamic behavior of composite rotors, this study focused mainly on the development of a numerical model for thick-walled composite shafts. This initial approach ignored the dynamic effects generated by rotary inertia and its related terms, for the necessity of initially focusing on the mechanical and physical properties of the composite and the associated numerical procedures, necessary for its correct formulation. It was noted that the damping coefficient was especially problematic to be modeled in thick walled shafts as the energy of the applied external excitation changed in amplitude, as became evident with preliminary experimental results and as studied with a different focus by (Wettergren, 1998) and (Singh and Gupta, 1996b). To implement a proper solution to the problem, the study emphasized the accurate determination of the modal damping coefficients and the development of a trustworthy methodology to do so.

2.1 Numerical formulation

The proposed FEM model aims to better represent a thick-walled composite hollow shaft, by using shell type elements. The formulation adopted in this work is based on the First Order Shear Deformation Theory (FSDT), with additional terms in the stiffness coefficients, similarly to what has been proposed by (Reddy, 2003) and (Reddy, 2002). The primary variables considered in the model are $(u_0, v_0, w_0, \phi_1, \phi_2)$, being three displacements and two rotations, following the coordinate system presented in Figure 1.

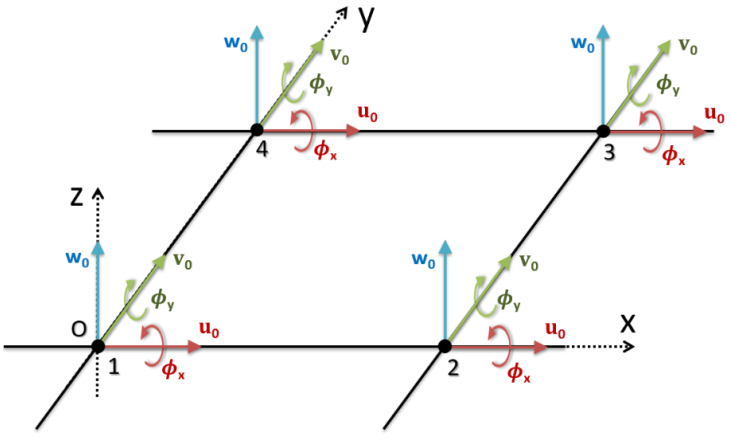

Figure 1: Bilinear shell type FE

The displacement equations on their weak form are presented below:

$$0 = \int_{\Omega^e} \left[\frac{\partial \delta u_0}{\partial x} N_1 + \frac{\partial \delta u_0}{\partial y} (N_6 + C_0 M_6) - \delta u_0 \frac{Q_1}{R_1} + I_0 \delta u_0 \frac{\partial^2 u_0}{\partial t^2} + I_1 \delta u_0 \frac{\partial^2 \phi_1}{\partial t^2} \right] dxdy - \oint_{\Gamma^e} P_1 \delta u_0 ds; \quad (1)$$

$$0 = \int_{\Omega^e} \left[\frac{\partial \delta v_0}{\partial x} (N_6 - C_0 M_6) + \frac{\partial \delta v_0}{\partial y} N_2 - \delta u_0 \frac{Q_2}{R_2} + I_0 \delta u_0 \frac{\partial^2 v_0}{\partial t^2} + I_1 \delta v_0 \frac{\partial^2 \phi_2}{\partial t^2} \right] dxdy - \oint_{\Gamma^e} P_2 \delta v_0 ds; \quad (2)$$

$$0 = \int_{\Omega^e} \left[\frac{\partial \delta w_0}{\partial x} Q_1 + \frac{\partial \delta w_0}{\partial y} Q_2 - \delta w_0 \left(\frac{N_1}{R_1} + \frac{N_2}{R_2} \right) - \delta q w_0 + I_0 \delta w_0 \frac{\partial^2 w_0}{\partial t^2} + \frac{\partial \delta w_0}{\partial x} \left(\widehat{N}_1 \frac{\partial w_0}{\partial x} + \widehat{N}_6 \frac{\partial w_0}{\partial y} \right) + \frac{\partial \delta w_0}{\partial y} \left(\widehat{N}_6 \frac{\partial w_0}{\partial x} + \widehat{N}_2 \frac{\partial w_0}{\partial y} \right) \right] dxdy - \oint_{\Gamma^e} V_n \delta w_0 ds; \quad (3)$$

$$0 = \int_{\Omega^e} \left[\frac{\partial \delta \phi_1}{\partial x} M_1 + \frac{\partial \delta \phi_1}{\partial y} M_6 + \delta \phi_1 Q_1 + I_2 \delta \phi_1 \frac{\partial^2 \phi_1}{\partial t^2} + I_1 \delta \phi_1 \frac{\partial^2 u_0}{\partial t^2} \right] dxdy - \oint_{\Gamma^e} T_1 \delta \phi_1 ds; \quad (4)$$

$$0 = \int_{\Omega^e} \left[\frac{\partial \delta \phi_2}{\partial x} M_6 + \frac{\partial \delta \phi_2}{\partial y} M_2 + \delta \phi_2 Q_2 + I_2 \delta \phi_2 \frac{\partial^2 \phi_2}{\partial t^2} + I_1 \delta \phi_2 \frac{\partial^2 v_0}{\partial t^2} \right] dxdy - \oint_{\Gamma^e} P_1 \delta \phi_2 ds; \quad (5)$$

where the constants and other variables are given by the following expressions:

$$C_0 = \frac{1}{2} \left(\frac{1}{R_1} - \frac{1}{R_2} \right); \quad (6)$$

$$P_1 \equiv N_1 n_1 + (N_6 + C_0 M_6) n_2; \quad (7)$$

$$P_2 \equiv N_2 n_2 + (N_6 - C_0 M_6) n_1; \quad (8)$$

$$T_1 \equiv M_1 n_1 + M_6 n_2; \quad (9)$$

$$T_2 \equiv M_6 n_1 + M_2 n_2; \quad (10)$$

$$V_n = \left(Q_1 + \widehat{N}_1 \frac{\partial w_0}{\partial x} + \widehat{N}_6 \frac{\partial w_0}{\partial y} \right) n_1 + \left(Q_2 + \widehat{N}_6 \frac{\partial w_0}{\partial x} + \widehat{N}_2 \frac{\partial w_0}{\partial y} \right) n_2; \quad (11)$$

which can also be assembled in matrix form:

$$\begin{Bmatrix} \{N\} \\ \{M\} \end{Bmatrix} = \begin{bmatrix} [A] & [B] \\ [C] & [D] \end{bmatrix} \begin{Bmatrix} \{\varepsilon^0\} \\ \{\kappa\} \end{Bmatrix} - \begin{Bmatrix} \{N\} \\ \{M\} \end{Bmatrix}^M; \quad (12)$$

$$\begin{Bmatrix} Q_2 \\ Q_1 \end{Bmatrix} = K_S \begin{bmatrix} A_{44} & A_{45} \\ A_{45} & A_{55} \end{bmatrix} \begin{Bmatrix} \varepsilon_4^0 \\ \varepsilon_5^0 \end{Bmatrix} - \begin{Bmatrix} Q_2^M \\ Q_1^M \end{Bmatrix}. \quad (13)$$

In the previous expressions, $\widehat{N}_1, \widehat{N}_2$ and $\widehat{N}_6$ are the applied surface loads. This methodology also allow for C^0 interpolation in the displacements, which ensures that there are no discontinuities in the displacements field along the thickness direction. This approach ultimately leads to results that are more accurate, which are most noticeable for the cases in which the thickness of the wall increases in thickness. One can now use interpolation functions of the form:

$$u_0(x, y, t) = \sum_{j=1}^{m} u_j(t) \psi_j^e(x, y), \quad (14)$$

$$v_0(x, y, t) = \sum_{j=1}^{m} v_j(t) \psi_j^e(x, y), \quad (15)$$

$$w_0(x, y, t) = \sum_{j=1}^{m} w_j(t) \psi_j^e(x, y), \quad (16)$$

$$\phi_1(x, y, t) = \sum_{j=1}^{m} S_j^1(t) \psi_j^e(x, y), \quad (17)$$

$$\phi_2(x, y, t) = \sum_{j=1}^{m} S_j^2(t) \psi_j^e(x, y), \quad (18)$$

where ψ_j^e are Lagrange interpolation functions. By substituting equations (14) through (18) in equations (1) through (5) and rearranging the ensuing terms into matrix form, the semi-discreet finite element model for the shell element using FSDT can be obtained:

$$\left(\begin{bmatrix} [K^{11}] & [K^{12}] & [K^{13}] & [K^{14}] & [K^{15}] \\ [K^{12}]^T & [K^{22}] & [K^{23}] & [K^{24}] & [K^{25}] \\ [K^{13}]^T & [K^{23}]^T & [K^{33}] & [K^{34}] & [K^{35}] \\ [K^{14}]^T & [K^{24}]^T & [K^{34}]^T & [K^{44}] & [K^{45}] \\ [K^{15}]^T & [K^{25}]^T & [K^{35}]^T & [K^{45}]^T & [K^{55}] \end{bmatrix} + \begin{bmatrix} [0] & [0] & [0] & [0] & [0] \\ [0] & [0] & [0] & [0] & [0] \\ [0] & [0] & [G] & [0] & [0] \\ [0] & [0] & [0] & [0] & [0] \\ [0] & [0] & [0] & [0] & [0] \end{bmatrix}\right) \begin{Bmatrix} \{u^e\} \\ \{v^e\} \\ \{w^e\} \\ \{S^1\} \\ \{S^2\} \end{Bmatrix} + \begin{bmatrix} I_0[M] & [0] & [0] & I_1[M] & [0] \\ [0] & I_0[M] & [0] & [0] & I_1[M] \\ [0] & [0] & I_0[M] & [0] & [0] \\ I_1[M] & [0] & [0] & I_2[M] & [0] \\ [0] & I_1[M] & [0] & [0] & I_2[M] \end{bmatrix} \begin{Bmatrix} \{\ddot{u}^e\} \\ \{\ddot{v}^e\} \\ \{\ddot{w}^e\} \\ \{\ddot{S}^1\} \\ \{\ddot{S}^2\} \end{Bmatrix} = \begin{Bmatrix} \{F^1\} - \{F^{T1}\} \\ \{F^2\} - \{F^{T2}\} \\ \{F^3\} \\ \{F^4\} - \{F^{T4}\} \\ \{F^5\} - \{F^{T5}\} \end{Bmatrix}, \tag{19}$$

which allows for the development of the modelling tool proposed on this paper.

2.2 Experimental validation

Regarding the experimental procedure, a composite hollow shaft was analyzed and its frequency response functions (FRFs) were obtained for the free-free condition. The shaft used is a thick walled hollow shaft made of a multi-layered carbon-epoxy composite. The shaft was suspended by its ends with two low rigidity elastic bands and an electrodynamic exciter was attached to it, allowing for external forces application, as schematically shown in figure 2.

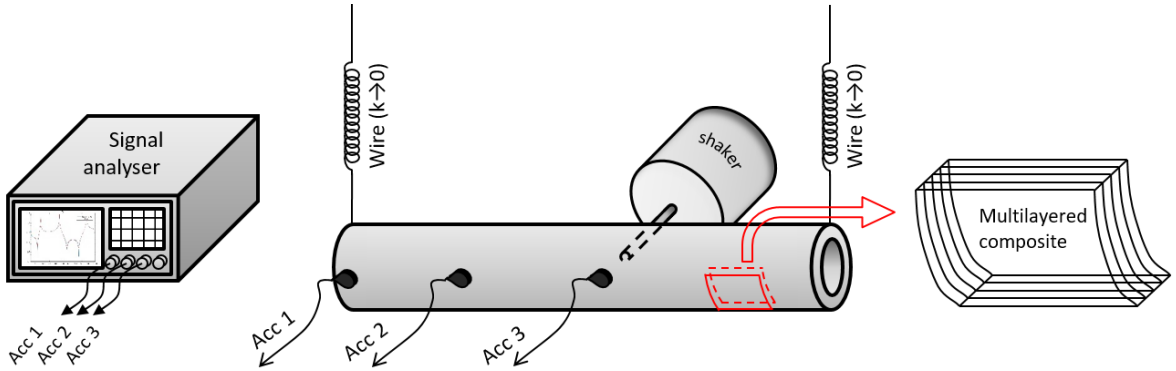

Figure 2: Experimental FRFs acquisition scheme

The shaft experimented on was manufactured using special high-modulus pre-impregnated carbon fibers, having twenty layers with the stacking sequence [0 0 0 0 90 90 45 -45 0 0 0 45 -45 90 90 0 0 0 0 0/90] going from the inner to the outer layers. The physical properties of the shaft are presented in Table 1, as provided by the manufacturer.

Table 1. Mechanical and geometrical properties of the composite shaft.

Property	Value
Length (m)	0.907
Outer diameter (m)	0.018
Internal diameter (m)	0.0128
Density (kg/m3)	1600
Young's Modulus 0° (GPa)	90,70
Young's Modulus 90° (GPa)	68,50
In-Plane Shear Modulus (GPa)	11,25
Major Poisson's Ratio	0.38

The experimental test rig is depicted in Figure 3.

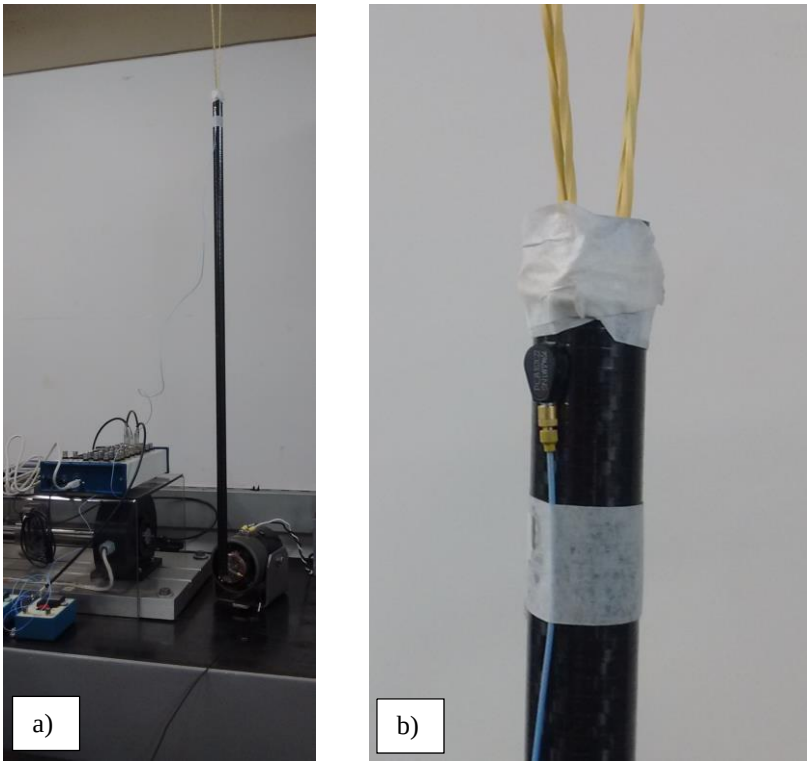

Figure 3: Experimental FRFs acquisition: a) Experiment overview; b) Accelerometer position.

These FRFs were obtained by applying different amplitude white noise through with the electrodynamic shaker, and acquiring the response using accelerometers in the positions depicted in Figure 2. The shaft is 907mm long, with all acquisition positions directly opposite to the shake placement, those being a) Node 1, ~0mm; b) Node 17, 378mm; c) Node 24, 529mm, being the last one in the same node of the shaker. The white noise applied varied in amplitude, ranging from 0.2N to 1.05N with a step of 0.05N, being intended to allow for proper model adjustment and validation, focusing on the modal damping factors.

2.3 Model adjustment via optimization procedure

Once the model was initially tested and the experimental results were obtained, the unknown parameters were adjusted by using Differential Evolution Optimization (Lobato and Steffen, 2008). Two sets of optimizations were performed, being one for the stiffness (*Young and Transversal modules*), *Mass* and the *Poisson Ratio*, and the second set that was exclusively dedicated to the three considered modal damping factors.

The primary optimization was performed for the 17 analyzed cases and the mean value of each unknown was adopted as "true" for all the cases in the second optimization set, as a standardizing procedure. During the second set, the damping modules were also updated for each individual experimental data set, without any averaging being performed in the end.

3. RESULTS AND DISCUSSION

The experimental results show that the methodology conveyed can properly represent the static behavior and the FRFs of a thick-walled composite shaft. As can be seen in figure 4, the model was able to predict the FRFs, as intended. This set of figures depict the final model result, after the two sets of optimizations, each having independently determined modal damping factors, showing perfect agreement between the experimental and theoretical results. It is also noteworthy that, when comparing analysis with different amplitudes of excitation, the results are almost exactly equal in their critical frequency amplitudes. For briefness, only 5 of the 17 sets of results are presented, as the results are visibly similar.

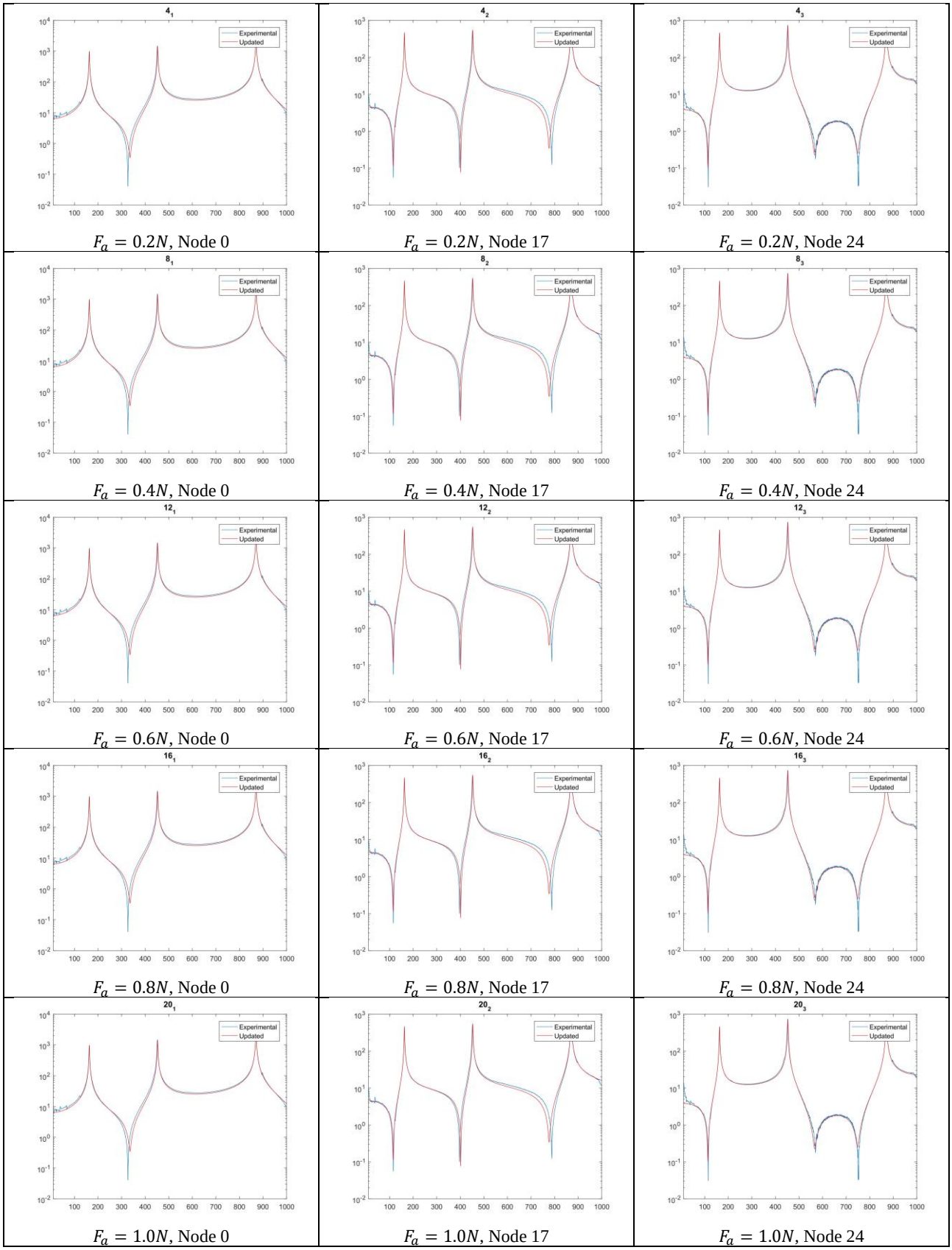

$F_a = 0.2N$, Node 0 | $F_a = 0.2N$, Node 17 | $F_a = 0.2N$, Node 24

$F_a = 0.4N$, Node 0 | $F_a = 0.4N$, Node 17 | $F_a = 0.4N$, Node 24

$F_a = 0.6N$, Node 0 | $F_a = 0.6N$, Node 17 | $F_a = 0.6N$, Node 24

$F_a = 0.8N$, Node 0 | $F_a = 0.8N$, Node 17 | $F_a = 0.8N$, Node 24

$F_a = 1.0N$, Node 0 | $F_a = 1.0N$, Node 17 | $F_a = 1.0N$, Node 24

Figure 4: Experimental and theoretical FRFs comparing results with different excitation amplitudes and accelerometer placement positions.

Also remarkable are the optimized values of the modal damping factors, which were determined independently for each set of experimental results, as shown in figure 5:

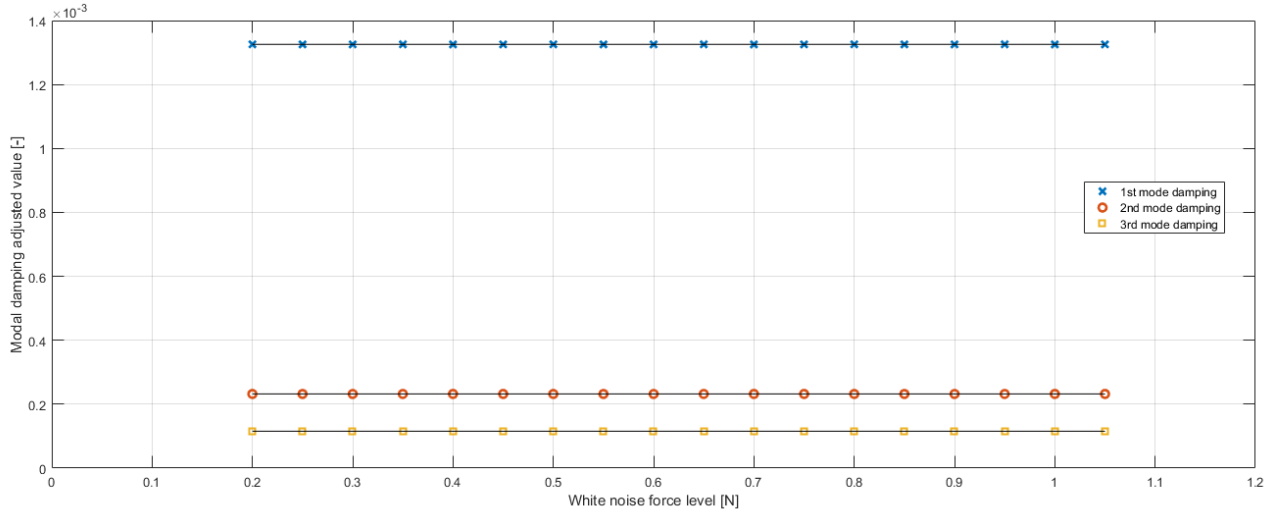

Figure 5: Optimized values of the three modal damping factors for each of the 17 different excitation amplitude tests.

4. CONCLUSIONS

As proposed, this paper presented an investigation dedicated to a numerical methodology for representing thick-walled composite hollow shafts. The proposed methodology is able to predict the behavior of the shaft satisfactorily, with special attention given to the modal damping factors.

As a remark, it is expected to have variable responses in terms of damping as the amplitude of the excitation increases; although this variation will only become considerable for high excitation levels. This high amplitudes were not attained by the tests performed. It is worth mentioning that future experimentation are schedule for the rotor shaft under operating conditions whose excitation level are well below the excitation used in the present contribution. The obtained results help to ensure safe operation of the machine, and also give a better understanding of the dynamic behavior of the system.

The procedure to determine the modal damping factors and general mechanical and physical properties was succesfully developed, as even for various levels of excitation performed during the experimental tests, the results obtained for the parameters were very satisfactory.

It is intended to expand this study by performing new experimentatal tests with rotating machinery using composite thick-walled shafts, particularly for further improving the numerical model. Currently, the composite shaft studied in the present contribution has been incorporated to a composite rotor system with rigid discs attached to the shaft, allowing for the observation of other dynamic effects and the development of more in-depth investigations.

5. ACKNOWLEDGEMENTS

The authors are thankful to the Brazilian Research Agencies FAPEMIG, CNPq (INCT-EIE), and CAPES for the financial support provided to this research effort.

6. REFERENCES

Alwan, V., Gupta, A., Sekhar, A.S., and Velmurugan, R., 2010. Dynamic analysis of shafts of composite materials. Journal of Reinforced Plastics and Composites 29: 3364-3379.

Cavalini Jr., A. A., Guimarães, A. M. T., Da Silva, B. R. M. G., Steffen Jr., V., (2017), “Analysis of the dynamic behavior of a rotating composite hollow shaft”, Latin American Journal of Solids and Structures, Vol. 14, pp. 1-16.

Chatelet, E., Lornage, D., and Jacquet-Richardet, G., 2002. A three dimensional modeling of the dynamic behavior of composite rotors. International Journal of Rotating Machinery 8: 185-192.

Crompton Technology Group Limited. Transmission Shafts. Website: <http://www.ctgltd.com/aerospacecomposites >. Accessed on: April 18th 2015

Ishida, Y. and Yamamoto, T., 2012. Linear and nonlinear rotordynamics. Wiley-VCH.

Lallement, G., Lecoanet, H., and Steffen Jr, V., 1982. Vibrations de rotors sur paliers à matrice de raideur non symetrique. Machine and Mechanism Theory 17: 47-55.

Lobato FS, Steffen V., 2008 Otimização multi-objetivo para o projeto de sistemas de engenharia Doc Thesis Universidade Federal de Uberlândia.

Nelson, H.D. and Macvaugh, J.M., 1976. The dynamics of rotor bearing systems using finite elements. Journal of Engineering for Industry 98: 593-600.

Reddy, J, N. Mechanics of laminated composite plates and shells: theory and analysis, CRC Press LLC, 2003.
Reddy, J, N. Energy Principles and Variational Methods in Applied Mechanics, John Wiley e Sons, 2002.
Ren, Y., Dai, Q., Na, R., and Zhu, Y. 2014. Modeling and dynamical behavior of rotating composite shafts with SMA wires. Shockand Vibration 2014: 1-16.
Singh, S.P. and Gupta, K., 1996a. Composite shaft rotordynamic analysis using a layerwise theory. Journal of Sound and Vibration 2: 179-186.
Singh, S.P. and Gupta, K., 1994b. *Free damped flexural vibration analysis of composite cylindrical tubes using bean and shell theories*. Journal of Sound and Vibration, Vol. 172, p. 171-190.
Sino, R., Baranger, T.N., Chatelet, E., and Jacquet-Richardet, G., 2008. Dynamic analysis of a rotating composite shaft. Composites Science and Technology 68: 337-345.
Wettergren, H. L., 1997, "Material Damping in Composite Rotors". In: Journal of Composite Materials, Vol. 32, No. 7/1998, Technomic Publishing Co., Inc.

7. RESPONSIBILITY NOTICE

The authors are the only responsible for the printed material included in this paper.